JOURNAL OF APPLIED POLYMER SCIENCE VOL. 14, PP. 1303–1321 (1970)

High Flux Freeze-Dried Cellulose Acetate Reverse Osmosis Membranes as Microporous Barriers in Gas Permeation and Separation

J. P. AGRAWAL and S. SOURIRAJAN, *Division of Chemistry, National Research Council of Canada, Ottawa*

Synopsis

The permeations of helium, hydrogen, methane, ethylene, nitrogen, and argon, and helium–methane, nitrogen–ethylene, oxygen–nitrogen, and sulfur dioxide–nitrogen mixtures have been studied using freeze-dried porous cellulose acetate reverse osmosis membranes. The results illustrate the existence of mobile and immobile sorbed layers and the governing influence of surface flow in gas-phase reverse osmosis separations. Preshrunk freeze-dried porous cellulose acetate membranes seem to offer a practical means of utilizing the reverse osmosis process for recovering helium from natural gas and separating sulfur dioxide from flue gases.

INTRODUCTION

The flow of gases through microporous media has been studied extensively.[1–3] Three major mechanisms govern the transport of gases through a microporous medium. They are free molecular flow (Knudsen flow), viscous flow, and surface flow. When the diameter of the pore is much less than the mean free path of the gas molecules, Knudsen flow predominates, under which conditions

$$R_{\text{eff}} = P_2 \left[\frac{N^2}{2\pi RTM}\right]^{1/2} \pi r^2 \tag{1}$$

where R_{eff} = molecular rate of effusion (molecules per sec), P_2 = absolute pressure of gas on the high pressure side of the porous medium, N = Avagadro number, R = gas constant, T = absolute temperature of gas, M = molecular weight of gas, and r = pore radius.[4] When the diameter of the pore is much more than the mean free path of the gas molecules, viscous or hydrodynamic flow predominates; for incompressible laminar isothermal viscous flow through a long cylindrical pore,

$$Q = \frac{\pi r^4}{8\eta l} (P_2^2 - P_1^2) \tag{2}$$

where Q = volumetric rate of gas permeation, η = coefficient of viscosity for the gas, l = effective length of pore, and P_1 = absolute pressure of the

atmosphere on the low pressure side of the membrane.[4] Thus the volume rate of gas permeation through a porous medium is proportional to r^2, P_2, $M^{-1/2}$, and $T^{-1/2}$ for Knudsen flow, whereas it is proportional to r^4, $(P_2^2 - P_1^2)$, and $1/\eta$ for incompressible laminar isothermal viscous flow. In general η is proportional to $\sqrt{T}$ for gases at low pressures. The phenomenon of sorption of gases on solid surfaces is well known, and the mobility of the sorbed layer and the contribution of surface flow to the total transport of material through the microporous medium have been extensively discussed.[1,2,5-9] In general, all the above three types of flow may be said to occur simultaneously in gas–solid systems involving microporous media.

With respect to the flow of gaseous mixtures through microporous media, Knudsen flow results in separation, but the degree of separation obtainable is limited by the molecular weight differences. Viscous flow involves no separation. The existence and mobility of a sorbed layer results in separation the extent of which depends on the chemical nature of the gas–solid system and the porous structure of the microporous medium and the other experimental conditions used. Preferential sorption on the membrane surface and the difference in the mobility of the sorbed layer compared to that of the bulk fluid through the membrane pores, together with gas phase Knudsen and/or viscous flow through the membrane pores, under pressure, constitute the basis for the applicability of the reverse osmosis technique for the separation of gases.[10,11] From this point of view, the permeation of several pure gases and gaseous mixtures through porous cellulose acetate reverse osmosis membranes has been studied in this work.

EXPERIMENTAL

Gases of 99.9% purity, supplied by Matheson of Canada Ltd., and CA-NRC-18-type porous cellulose acetate membranes made in the laboratory by the method described by Sourirajan and Govindan[12] were used. These membranes are usually 0.004 in. thick and have a relatively dense microporous structure (pore size $\sim$50 Å or more) on an extremely thin layer ($\sim 10^{-5}$ in.) of the membrane surface which was exposed to the atmosphere during casting. The remainder of the membrane material underneath this thin surface layer is a spongy, porous mass containing comparatively very big pores ($\sim$4000 Å). Consequently the above membranes are said to have an asymmetric porous structure. The above pore sizes can be reduced by shrinking the membranes by simply keeping them immersed in hot water for about 10 min. Thus by adjusting the temperature of hot water during shrinking, different pore sizes on the surface layer side of the membrane can be obtained. It is the microporous structure of the dense surface layer which governs the level of reverse osmosis separation and hence is held in contact with the feed fluid during operation.[14]

The experiments were carried out in the reverse osmosis cell illustrated in Figures 1 and 2. The cell was a stainless steel pressure chamber consist-

ing of two detachable parts. The film was mounted on a stainless steel porous plate embedded in the lower part of the cell through which the membrane-permeated liquid or gas was withdrawn at atmospheric pressure. The upper part of the cell contained the feed gas or solution under pressure in contact with the membrane. The two parts of the cell were clamped and sealed tight with rubber O-rings. The feed gas or solution was kept well stirred by means of a magnetic stirrer fitted in the cell about $^1/_4$ in. above the membrane surface. The cell was also provided with an external heating tape or cooling jacket and an internal thermocouple. Most of the experiments were carried out at laboratory temperature (~24°C), but a few experiments were also carried out at higher and lower temperatures. Membranes shrunk at different temperatures and capable of giving different levels of solute separations in reverse osmosis experiments using aqueous

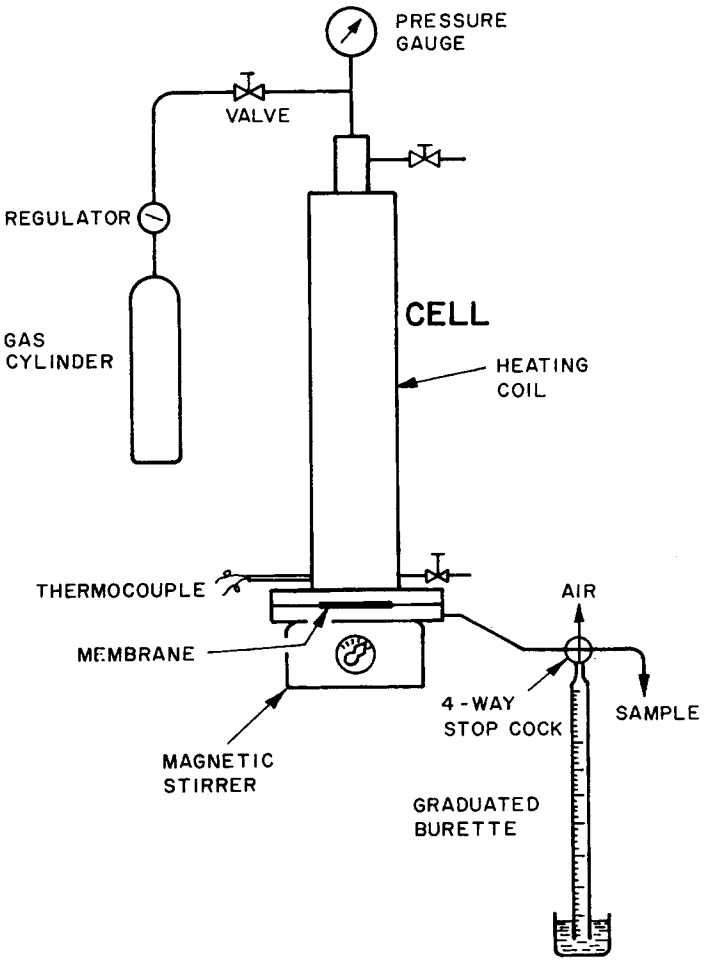

Fig. 1. Reverse osmosis cell assembly.

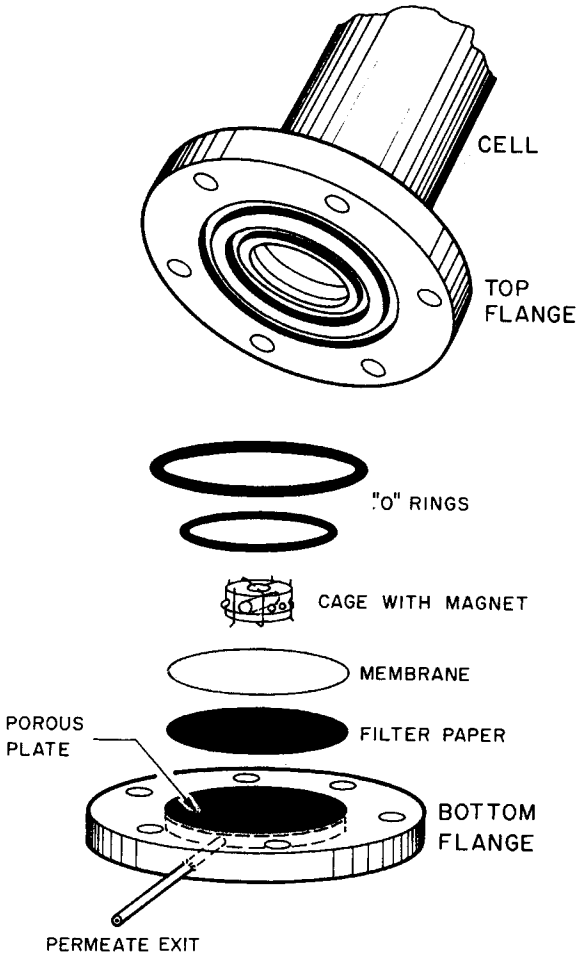

Fig. 2. Reverse osmosis cell details.

sodium chloride feed solutions were used. The following procedure was repeated for each membrane.

The preshrunk membrane was pressurized at 750 psig under water at laboratory temperature for 1 hr. The membrane was allowed to relax for several hours after releasing this pressure. This initial pressurization is required for stabilized and reproducible membrane performance. Next, a complete wet run was done which consisted of measuring the pure water permeability (PWP), product rate (PR), and solute separation (f), at 600 psig and laboratory temperature using 0.5 wt-% NaCl aqueous feed solution. The above data were used to obtain the specifying parameters for the film expressed in terms of the pure water permeability constant A and the solute transport parameter ($D_{AM}/K\delta$) for NaCl at 600 psig; these parameters were calculated using the Kimura-Sourirajan analysis.[13,14] After the

wet run, the membrane was again allowed to relax for a few hours at atmospheric pressure, after which time it was freeze dried as follows.

The wet membrane was immersed in a small volume of isopentane precooled at Dry Ice temperature (~−80°C) followed by overnight vacuum drying at the same temperature; the membrane was finally vacuum dried at −10°C using a glycol–water bath for cooling. A vacuum of about 500 μ was maintained throughout. This two-step freeze-drying technique retained the flexibility of the membrane which was essential for its convenient use in gas permeation experiments.

The freeze-dried membrane was used for all gas permeation experiments. The membrane-permeated gas was collected over water at laboratory temperature and atmospheric pressure (Fig. 1). When gaseous mixtures were used as feed, the compositions of the feed and product gases were determined by gas chromatographic analysis, details of which are given along with Table III. The gas permeation rates were reproducible within 2% in all cases. A maximum error of 2% in absolute concentrations (~5% in the case of some dilute sulfur dioxide mixtures) was estimated for the results of chromatographic analysis; this error, however, is essentially cancelled in the calculation of separation factors. Each experiment was repeated at least three times to ensure the accuracy of the separation factors and gas permeation rates reported. On completion of the gas permeation experiments, the wet reverse osmosis run was repeated with the membrane and the results were compared with those obtained before freeze drying.

RESULTS AND DISCUSSION

Effect of Freeze Drying on the Porous Structure of Membranes

Table I gives the performance of several films before and after freeze drying in reverse osmosis experiments using 0.5 wt-% NaCl aqueous feed solutions under the same experimental conditions. Films G5 and G19 were preshrunk at the same temperature; film G5 was air dried and film G19 was freeze dried. A comparison of data for film G19 (before and after freeze drying) with those for the air-dried film G5 shows that air drying shrinks the surface pore size and collapses the bulk porous structure of the membrane, resulting in much higher solute separations and very much lower product rates. On the other hand, freeze drying also shrinks the surface pore size to some extent as seen from an increase in solute separation from 68.0 to 80.9%; but the product rate obtained with the freeze-dried membrane is reasonable for that level of solute separation, indicating thereby that freeze drying does not collapse the porous structure of the membrane as much as air drying does. The data for film G17A show that for highly shrunk membranes the change in pore structure brought about by freeze drying is even less. Thus it seems reasonable to conclude that the freeze drying technique used in this study preserves largely, though not com-

pletely, the porous structure of the reverse osmosis cellulose acetate membranes.

Permeation of Pure Gases

Effects of Pressure, Temperature, Nature of Gas and Pore Size on Membrane Surface

Figures 3 and 4 illustrate the above effects on the gas permeability constant A_G, expressed as (g mole of gas)/(cm^2 sec atm), using a few typical freeze-dried membranes of different porosities. The average pore size on the membrane surface is highest for film G16A and lowest for film G22, the pore size for the other films used being in between, as is evident from their respective A and $(D_{AM}/K\delta)$ values given in Table I.

At constant temperature and pressure, the values of A_G for various gases are in the order He > CH_4 > C_2H_4 > N_2, both for film G16A (Fig. 3) and film G22 (Fig. 4). This order, however, is not strictly maintained for all the films and, further, the values of A_G are not strictly inversely proportional to the square root of the molecular weight of the gases. These results indicate the existence of gas sorption and the governing influence of surface flow in the reverse osmosis membrane used.

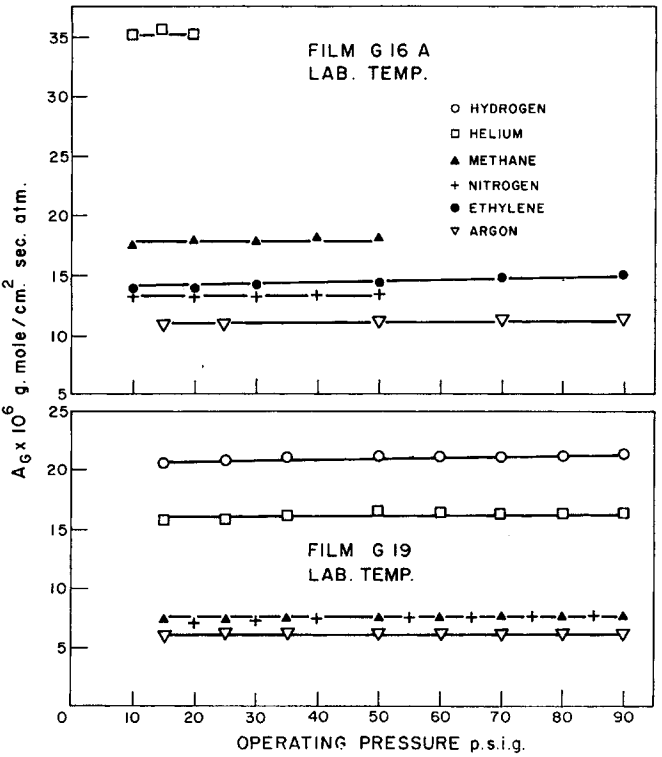

Fig. 3. Data on permeation of pure gases.

TABLE I
Membrane Specifications and Performance of Membranes Before and After Freeze Drying[a]

Film no.	Shrinkage temp, °C	Before freeze drying[b] [PWP], g/hr	[PR], g/hr	f, %	A $\times 10^5$	$(D_{AM}/K\delta)$ $\times 10^5$	After freeze drying [PWP], g/hr	[PR], g/hr	f, %
G5[c]	85	—	—	—	—	—	1.38	1.23	98.0
G16A	80	253	196	32	9.72	156.7	—	—	—
G17A	90	34.1	28.7	96.5	1.31	1.70	28.3	26.6	97.8
G17B[d]	90	25.6	22.0	98.2	0.98	0.76	—	—	—
G18[d]	95	8.2	7.4	>99.0	—	—	—	—	—
G19	85	99.6	85.1	68.0	3.83	49.9	71.6	56.3	80.9
G22[d]	92	11.1	10.0	98.6	0.43	0.55	—	—	—
G23	95	10.2	9.2	>99.0	—	—	—	—	—

[a] Film type, CA-NRC-18; system, NaCl–H_2O; feed concentration, 0.5 wt-% NaCl; operating pressure, 600 psig; film area, 9.6 cm^2.
[b] A, Pure water permeability constant in (g mole H_2O)/(cm^2 sec atm); $(D_{AM}/K\delta)$, solute transport parameter in cm/sec.
[c] Film air dried at laboratory temperature.
[d] Film surface damaged after a few experiments.

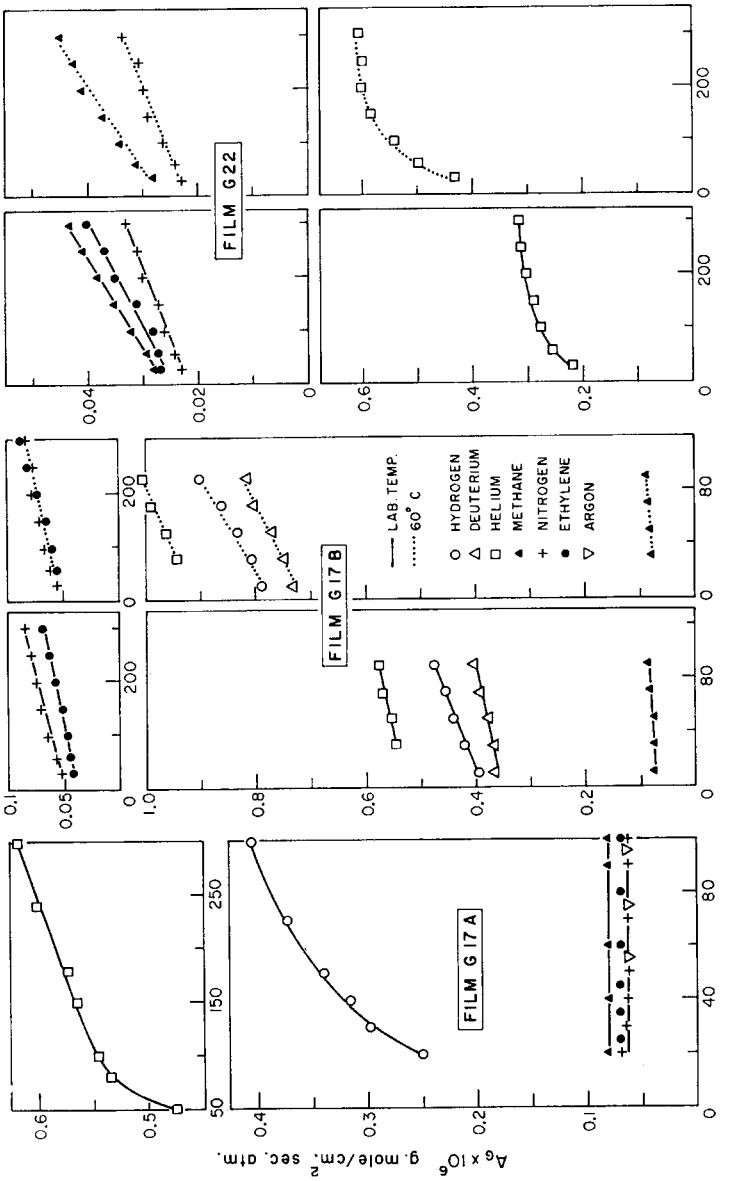

Fig. 4. Data on permeation of pure gases.

At the laboratory temperature, A_G for He, CH_4, C_2H_4, N_2, and argon is essentially independent of operating pressure up to 90 psig for film G16A. These results indicate that gas permeation is essentially free molecular in nature even with respect to the most porous membrane studied. The A_G tends to increase with operating pressure as the pore size on the membrane surface decreases. This effect is most predominant for He and H_2 and far less for the heavier gases CH_4, C_2H_4, N_2, and argon. These results indicate that while it is only reasonable to expect higher sorption at higher operating pressures, the sorbed layer is also relatively much more mobile at higher operating pressures, helium is most weakly sorbed on the membrane surface compared to other gases, and the effect of pressure on the mobility of the sorbed layer is very much more with respect to weakly sorbed gases.

Figure 4 shows that a higher operating temperature tends to increase the mobility of the sorbed layer and hence A_G. But the magnitude of this effect depends again on the chemical nature of the gas with respect to that of the membrane. While the values of A_G for He, H_2, and D_2 increased significantly by increasing the operating temperature from ~24°C to 60°C, there was practically no change in the corresponding values of A_G for CH_4, C_2H_4, and N_2. These data indicate that the latter gases are more strongly sorbed on the membrane surface.

Average Size of Pores on Membrane Surface

When (r/λ) is small, where r is pore radius and λ is mean free path of gas molecules, Dushman[15] showed that gas flow would be mostly free molecular in nature. For example, when $(r/\lambda) = 0.1$, about 98% of total flow is said to be free molecular, and even when $(r/\lambda) = 1$, 85% of total flow is said to be free molecular. Liepmann,[16] on the other hand, showed by means of theoretical analysis that when $(2r/\lambda) = 0.1$, the deviation from free molecular flow would be about 1%. Liepmann's formulation seems generally accepted.[17]

Liepmann's analysis[16] offers a means of determining the average pore size on the surface of reverse osmosis membranes. This was done for a few cases by plotting volume rate of gas flow versus operating gauge pressure (Fig. 5) and determining the pressure at which the deviation from linear relationship exceeds 1%. At this pressure it is assumed that $(2r/\lambda) = 0.1$. It is implicit in this assumption that any nonlinearity in a graph of the type shown in Figure 5 is entirely due to the deviation from Knudsen flow, even in the presence of surface flow, and the effect of surface flow is only to give a lower value for the pore diameter than its real value.

The values of λ at the corresponding absolute pressure were calculated from data in the literature.[18] The pore diameters calculated from the above relationships based on the permeation rates of different gases are given in Table II for three membranes. In view of the uncertainties involved in the method of calculating pore diameters, the data given in Table II must be considered as only very approximate. Nevertheless, their order of magnitude is interesting. The method yields different pore di-

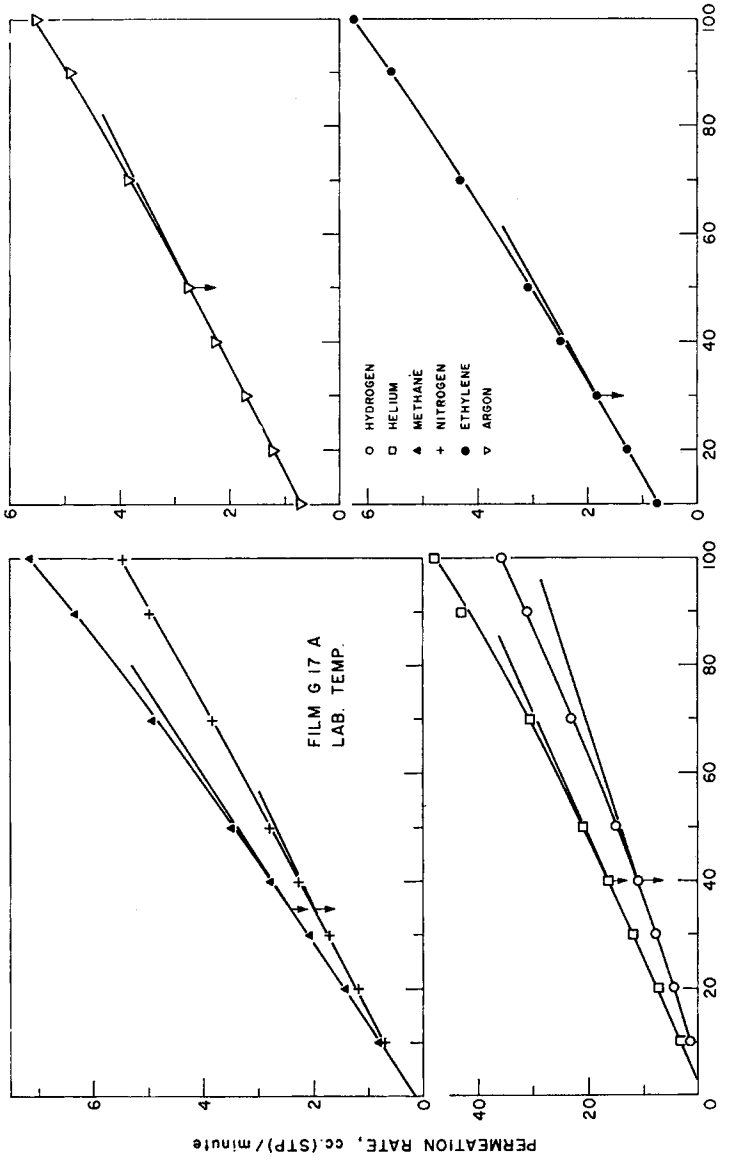

Fig. 5. Gas permeation rate vs. operating pressure.

ameters for the same membrane calculated from data on the permeation of different gases. This result indicates the partial blocking of the pores due to the relatively immobile sorbed layer at low operating pressures. In all cases, the pore diameter calculated from helium data is the greatest, indicating that the blocking effect of helium due to sorption is the least. The actual pore sizes should be greater than those obtained from the helium permeability data, i.e., larger than 38 Å and 35 Å for membranes G17A and G17B, respectively. These data agree with the work of Schultz and others[19] who calculated an average pore diameter of 44 Å for similar membranes from electron micrograph data.

TABLE II
Estimated Average Pore Diameters for Preshrunk Cellulose Acetate Membranes at Laboratory Temperature

Film no.	Average pore diameters, Å, based on permeation rates of pure gases					
	He	H_2	CH_4	N_2	C_2H_4	Argon
G17A	38	35	26	18	9	—
G17B	35	32	26	24	27	24
G22	14	—	9.5	9.1	6.4	—

Surface Flow and Gas Phase Flow

The term surface flow refers to the flow of the sorbed layer through the membrane pores, and the term gas phase flow refers to the free molecular and/or viscous flow through the membrane pores unhindered by surface effects. The experimental data presented above offer a means of analyzing the possible effects of sorption on gas permeation and the relative magnitudes of surface flow and gas phase flow through reverse osmosis membranes. With reference to any gas, the effect of sorption is to reduce the effective average pore diameter of the membrane for gas phase flow. Since sorption is present in all cases to some extent, the analysis can only be in relative terms. For the purpose of this analysis, helium is taken as the reference gas (since it is the most weakly sorbed gas on the membrane surface) and the gas phase flow is assumed free molecular. Thus, for any particular membrane, let d_{He} and d_G be the effective pore diameters with reference to helium and the particular gas under consideration, respectively. Following the Sourirajan mechanism[10] of reverse osmosis,

$$d_G = d_{He} - 2n\,\sigma_G \tag{3}$$

where n is the molecularity of the sorbed layer and σ_G is the molecular diameter of the gas.

The observed gas permeability coefficient A_G may be considered as the sum of two such coefficients $A_{G,SF}$ and $A_{G,GF}$ representing those due to surface flow and gas phase flow, respectively. Thus,

$$A_G = A_{G,SF} + A_{G,GF}. \tag{4}$$

Since the magnitude of gas phase flow is directly proportional to the effective area of the pore and inversely proportional to the square root of the molecular weight of the gas,

$$A_{G,GF} = A_{\mathrm{He}} \sqrt{\frac{M_{\mathrm{He}}}{M_G}} \left(\frac{d_G}{d_{\mathrm{He}}}\right)^2 \tag{5}$$

where A_{He}, M_{He}, and M_G represent the permeability coefficient for helium, molecular weight of helium, and molecular weight of gas, respectively. Defining

$$A_{G,\mathrm{He}} = A_{\mathrm{He}} \sqrt{\frac{M_{\mathrm{He}}}{M_G}}, \tag{6}$$

eq. (4) becomes

$$A_G = A_{G,SF} + A_{G,\mathrm{He}} \left(\frac{d_G}{d_{\mathrm{He}}}\right)^2. \tag{7}$$

Using eq. (3),

$$A_G = A_{G,SF} + A_{G,\mathrm{He}} \left(1 - \frac{2n\ \sigma_G}{d_{\mathrm{He}}}\right)^2 \tag{8}$$

or

$$\frac{A_G}{A_{G,\mathrm{He}}} = \frac{A_{G,SF}}{A_{G,\mathrm{He}}} + \left(1 - \frac{2n\ \sigma_G}{d_{\mathrm{He}}}\right)^2. \tag{9}$$

The quantity $(A_G/A_{G,\mathrm{He}})$ represents the ratio of the total observed permeation to the hypothetical gas phase permeation calculated from eq. (6) on the basis of the experimental helium permeability coefficient. This quantity is plotted in Figure 6 for several gases for three typical films, G19, G17A, and G22, whose average pore diameters (based on helium permeation data) are 54, 38, and 14 Å, respectively. Figure 6 shows the effects of the chemical nature of the gas with respect to that of the membrane material, operating pressure and temperature, and the porosity of the membrane surface on the parameter $(A_G/A_{G,\mathrm{He}})$. It may be seen that the magnitude of the above parameter is equal to, greater than, or less than 1, depending on experimental conditions; further, it decreases, increases, or remains constant as a function of operating pressure and temperature. These observations are entirely consistent with the forms of eqs. (8) and (9).

For example, when $d_{\mathrm{He}} \gg 2n\ \sigma_G$, i.e., for very large pore diameter and/or very low surface coverage, eq. (8) tends to become

$$A_G = A_{G,SF} + A_{G,\mathrm{He}} \tag{10}$$

in which case $(A_G/A_{G,\mathrm{He}})$ is greater than 1, as it observed in the case of argon, C_2H_4, and N_2 for film G19. On the other hand, when $d_{\mathrm{He}} \approx 2n\ \sigma_G$, i.e., for very small pore diameter and/or very high surface coverage, eq. (8) tends to become

$$A_G = A_{G,SF} \tag{11}$$

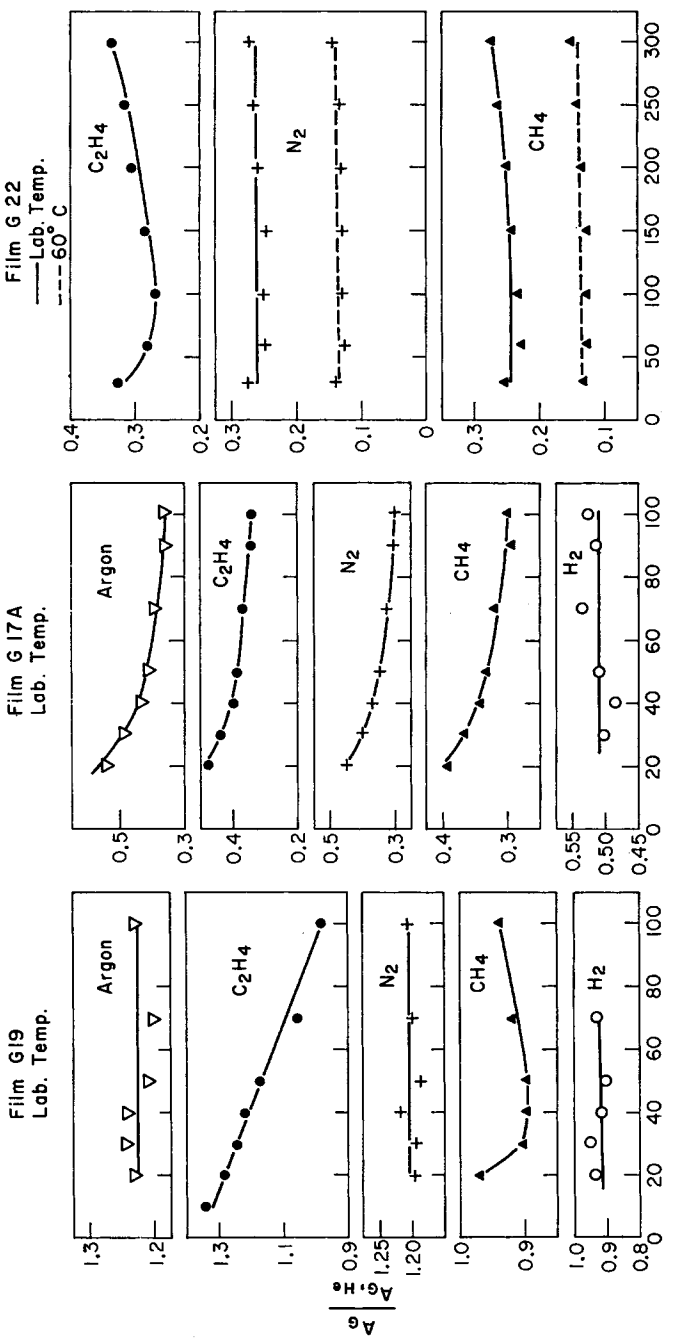

Fig. 6. Effect of surface flow on permeation rate of pure gases.

which means that the observed permeation is entirely due to surface flow. The data for films G17A and G22 show that $(A_G/A_{G,He})$ is less than 1 in all cases studied, which indicates that the magnitude of surface flow is always less than that of gas phase flow through an equivalent pore. In other words, the mobility of gas in the sorbed layer is always less than that in gas phase flow. The sorbed layer may in fact consist of both immobile and mobile parts. This possibility is indicated by the following illustrative calculations. Referring to data of CH_4 for film G17A, the value of $(A_G/A_{G,He})$ at 20 psig is 0.4. Assuming σ_G for methane is 4 Å, and $d_{He} = 38$ Å, one can calculate that the values of $(A_{G,SF}/A_G)$ are -0.56, 0.16, 0.66, and 0.94, respectively, for $n = 1$, 2, 3, and 4, using eqs. 3, 4, and 9. A negative value for $A_{G,SF}$ when $n = 1$ indicates the existence of an immobile monomolecular layer. One may make similar calculations at higher pressures also to illustrate the possible existence of multimolecular immobile sorbed layer, but it may not be reasonable to assume a constant d_{He} value in such calculations. In any case, the data presented in Figure 6 illustrate the significance of surface flow in gas permeation through reverse osmosis membranes.

Permeation and Separation of Gas Mixtures

Four binary gas mixtures which included helium–methane, nitrogen–ethylene, oxygen–nitrogen, and sulfur dioxide–nitrogen systems were studied. The system He–CH_4 is of interest from the point of view of the practical recovery of helium from natural gas; the system N_2–C_2H_4 is of interest in view of the equal molecular weight of gases involved; the system O_2–N_2 is of interest from the point of view of oxygen enrichment of air; and the system SO_2–N_2 is of interest from the point of view of air pollution control. The gas fluxes expressed as liters (STP) per square foot per hour and separation factors defined as

$$S = \left(\frac{X_A}{X_B}\right)_{\text{product}} \Big/ \left(\frac{X_A}{X_B}\right)_{\text{feed}}$$

where X_A and X_B are the mole fractions of **A** and **B** in the binary system **A–B**, were determined. A set of experimental results is given in Table III.

System Helium–Methane

Most of the experiments were carried out at the laboratory temperature; a few experiments were carried out at -80°C and also in the temperature range 55° to 64°C. The operating pressures were in the range 10 to 600 psig, and helium concentration in feed varied in the range 0.34 to 82.5 mole-%. Six membranes of different porosities (Table I) were used in this study. In all experiments except one (film G17A, -80°C, 10 psig, 31% He is feed), the membrane-permeated product was enriched in helium.

The observed separation factors (S), however, were always less than those (S_{AB}) calculated from the relation

$$S_{AB} = \frac{A_{G,A}}{A_{G,B}} \tag{12}$$

where $A_{G,A}$ and $A_{G,B}$ are the permeability coefficients for the pure gases **A** and **B**, respectively, under identical operating conditions of pressure and temperature. Further, the observed flux for the gas mixture was only 65% to 85% of $\Sigma X_i[PR]_i$, where X_i and $[PR]_i$ represent, respectively, the mole fraction of gas in the feed and permeation rate of pure gas at the same operating pressure and temperature. These results indicate that methane is preferentially sorbed and transported through the membrane, and the effective pore diameters for the individual gases in the mixture are less than those for the respective pure gases.

The separation factor and total flux through the membrane increased with increase in operating pressure, temperature, and helium concentration in feed. These data are consistent with the data given in Figures 3 and 4 for pure gases. An increase of operating pressure may be expected to increase both sorption and the mobility of the sorbed layer. Since these two changes may have opposing effects on separation factor depending on the other experimental conditions of feed concentration, operating temperature, and porosity, an optimum operating pressure for maximum separation factor may be expected for specific experimental conditions.

An increase in operating temperature increases the mobility of the sorbed layers, but the effect is much more with respect to helium (Fig. 4) resulting in higher separation factors. When the operating temperature is reduced to −80°C, the critical temperature of methane is approached, under which condition methane may be expected to behave more like a vapor, which means higher transport of methane through the membrane. Further, at low operating temperatures, the mean free path of molecules is smaller, under which condition free molecular flow will tend to change to viscous, and hence nonseparative, flow. Both the above effects result in a decrease in separation factor as observed; and, at least in one case (film G17A, −80°C, 10 psig, 31% He in feed), this decrease was sufficient to cause an enrichment of methane in the membrane-permeated product.

The possible existence of an immobile surface layer and the reduced mobility of sorbed layers have been pointed out; as a consequence, the effective pore size for methane, relative to that for helium, is steeply reduced on reducing the average pore size on the membrane surface. This accounts for the steep increase in separation factors obtained with highly preshrunk membranes.

With a helium concentration of 0.49 mole-% in feed, a separation factor of 8.6 and a flux of 72.6 liters (STP) per square foot per hour with a permeability coefficient of 47.4×10^{-9} (g mole of gas)/(cm^2 sec atm) were obtained at 300 psig and 57°C using film G22; with a helium concentration of 80 mole-% in feed, a separation factor of 8.2 and a flux of 155.6 liters (STP)

TABLE III

Reverse Osmosis Separation of Gaseous Mixtures Using Freeze-Dried Porous Cellulose Acetate Membranes[a]

System A–B	Film no.	Concn of A in feed	Operating conditions: Pressure, psig	Operating conditions: Temp, °C	Flux, (liter STP)/-(ft² hr)	$A_G \times 10^6$, (g mole)/-(cm² sec atm)	Observed separation factor S	S_{AB}
		Mole %						
He-CH_4	G17A	31	10	−80	*	*	0.86	
		33.5	50	Lab	*	*	2.7	6.06
		33	50	64	*	*	4.3	
		35	50	60	*	*	4.0	
		44.5	50	60	*	*	4.3	
		48	50	−80	*	*	1.12	
	G17B	0.55	50	Lab	13.3	52.4	3.0	7.3
		0.35	50	59	15.7	61.5	3.5	12.3
		0.34	150	59	64.4	84.2	4.4	
		0.41	215	58	106.2	96.9	4.1	
		26.5	50	Lab	43.0	168.5	4.5	
		26.4	50	58	54.0	211.8	5.5	
		84.0	50	Lab	90.6	355	4.9	
		80.0	50	57	155.6	610	8.2	
		79.4	150	61	493	645	7.2	
	G18	41.6	100	Lab	41.8	82.0	11.4	
	G22	0.49	300	57	72.6	47.4	8.6	13.4
		0.60	100	57	18.0	35.3	5.7	15.8
		21.5	100	57	53.4	104.8	9.1	
		34.0	100	57	79.0	154.8	10.5	
		82.5	40	55	66.2	324.0	8.8	
	G23	0.6	600	Lab	75.5	24.7	10.0	
		0.7	415	Lab	45.3	21.4	9.2	
		34.0	100	Lab	28.4	55.8	8.5	
	G19	0.6	10	Lab	54.0	1060	1.1	2.0

N_2–C_2H_4	G17A	48.0	50	Lab	15.2	59.2	1.2	
		49.0	100	Lab	29.4	57.7	1.05	
	G17B	48.0	100	Lab	29.6	58.1	1.13	1.46
		49.0	200	Lab	72.0	70.6	1.06	1.30
O_2–N_2	G17A	16.0	50	Lab	14.5	56.9	1.13	
		ppm						
SO_2–N_2	G23	670–820	200	Lab	12.4	12.2	5.2	
		5400–7600	200	Lab	15.1	14.8	13.8	
		5200–6700	200	Lab	16.1	15.9	10.4	
		18500	200	Lab	12.8	13.1	7.1	
		570–770	300	Lab	20.1	13.1	9.5	
		770–970	300	Lab	20.3	13.3	9.1	
		15800–18500	300	Lab	23.5	15.4	11.8	
		14200	370	Lab	30.2	16.0	15.2	
		950–1250	400	Lab	29.1	14.3	9.1	
		12800–13900	400	Lab	33.7	16.1	15.2	
		930–1150	500	Lab	38.5	15.1	10.3	
	G19	7500	10	Lab	56	1100	1.4	
Flue gas	G23	200	300	Lab	25.8	16.6	9.0	
(synthetic)		240	450	Lab	43.3	18.9	10.4	
		240	600	Lab	65.4	21.4	10.2	

[a] Notes: * means not determined. Lab means laboratory temperature, ~24°C. Flue gas composition: N_2:83.88, oxygen:5.9, CO_2:10.2, and SO_2:0.02%.

For flue gas, $S = \left(\frac{X_{SO_2}}{1 - X_{SO_2}}\right)_{product} \div \left(\frac{X_{SO_2}}{1 - X_{SO_2}}\right)_{feed}$.

Gas chromatography (thermal conductivity detector was used in all analysis):

He–CH_4, and air analysis: molecular sieve column; carrier gas argon or hydrogen; carrier gas flow rate 50 cc/min; column temp = 40°C: N_2–C_2H_4 analysis: Chromosorb column; carrier gas hydrogen; carrier gas flow rate 50 cc/min; column temp = 100°C. SO_2–N_2 anlyasis· column 30% dioctyl isocebacate on C22 firebrick; carrier gas helium; carrier gas flow rate 37 cc/min; column temp = 130°C. Flue gas analysis: molecular s'eve column in conjunction with column used for SO_2–N_2.

per square foot per hour with a permeability coefficient of 610×10^{-9} (g mole of gas)/(cm^2 sec atm) were obtained at 50 psig and 57°C using film G17B. These data may be compared with those given earlier[20] and the corresponding data of Stern and others[20] who obtained a separation factor of 7.3 and a flux of 3.71 liters (STP) per square foot per hour with a permeability coefficient of 0.81×10^{-9} (g mole of gas)/(cm^2 sec atm) at 900 psig and 80°C using 0.4 to 72 mole-% helium and a nonporous Teflon FEP film. The data presented in this paper indicate the practical possibility of recovering helium from natural gas economically by permeation under pressure through freeze-dried reverse-osmosis porous cellulose acetate membranes of the type employed in this work.

Other Systems

In the N_2–C_2H_4 system, the membrane-permeated product was enriched in nitrogen under the conditions of the experiment given in Table III; the observed separation factors were low and always less than S_{AB}. These data indicate the preferential sorption of ethylene on the membrane surface and the slow nature of surface flow. The fact that the operating temperature was not much higher than the critical temperature of ethylene (9.7°C) also contributes to the increased transport of ethylene and a consequent decrease in separation factor with respect to nitrogen.

In the O_2–N_2 system, the membrane-permeated product was enriched in oxygen even though it is a heavier gas, as is generally the case with all polymer membranes. The separation factor of 1.13 observed in this work is consistent with similar results obtained earlier by Sourirajan with Schleicher and Schuell membranes.[11]

At the laboratory temperature, sulfur dioxide is below its critical temperature (157.2°C), and hence it behaves as a vapor in reverse osmosis experiments. Thus, in the SO_2–N_2 system (Table III), the product was always enriched in SO_2 and the separation factors obtained were high. An increase in operating temperature from laboratory temperature to 60°C decreased the separation factor from 13.8 to 10.4 at 200 psig, using 5200 to 7600 ppm SO_2 in feed. Table III also gives some data on SO_2 separation, using a synthetic flue gas feed containing 200 to 240 ppm of SO_2. With membrane G23, SO_2 separation factors in the range 5.2 to 15.2 in one stage, and total fluxes in the range 12.4 to 65.4 liters (STP) per square foot per hour were obtained at laboratory temperature in the operating pressure range 200 to 600 psig, using feed concentrations in the range 200 to 18,500 ppm of SO_2. These results may be of practical interest in air pollution control and sulfur recovery.

CONCLUSIONS

The applicability of the reverse osmosis process for gas separations has been illustrated. Here again, as in liquid phase separations, the transport mechanism is governed by the chemical nature of the gas with respect to that of the membrane material, as well as the porous structure of the mem-

brane surface. In addition, the existence of mobile and immobile sorbed layers, relative mobility of the sorbed gas compared to gas phase flow, the relative condensibility of the gases in the mixture, and the mean free path of the molecules in the gas phase under the operating conditions of the experiment govern the separation factors and fluxes obtainable in the process. The osmotic pressure and concentration polarization effects are far less severe in gaseous systems than in systems in liquid phase. Freeze-dried porous cellulose acetate membranes of the type used in this work offer a means of utilizing the reverse-osmosis gas separation process for practical purposes such as the recovery of helium from natural gas.

The authors are grateful to Lucien Pageau and A. G. Baxter for their valuable assistance in the progress of these investigations. One of the authors (J. P. A.) thanks the National Research Council of Canada for the award of a postdoctoral fellowship.

Issued as N.R.C. No. 11294.

References

1. K. Kammermeyer, in *Progress in Separation and Purification*, Vol. 1, E. S. Perry, Ed., Interscience, New York, 1968, p. 335.

2. R. M. Barrer, *A. I. Ch. E.—I. Chem. E.* (London), *Symp. Ser.*, **1**, 112 (1965).

3. G. R. Youngquist, ACS Symposium on *Flow-Through Porous Media*, Washington, D.C., June 9–11, 1969.

4. A. D. Kirk, *J. Chem. Ed.*, **44**, 745 (1967).

5. S. Hwang and K. Kammermeyer, *Can. J. Chem. Eng.*, **44**, 82 (1966).

6. G. W. Sears, *J. Chem. Phys.*, **22**, 1252 (1954).

7. T. L. Hill, *J. Chem. Phys.*, **25**, 730 (1956).

8. W. D. Harkins and G. Jura, *J. Amer. Chem. Soc.*, **66**, 1356 (1944).

9. J. R. Dacey, in *Chemistry and Physics of Interfaces*, American Chemical Society, Washington, D.C., 1965, p. 151.

10. S. Sourirajan, *Ind. Eng. Chem., Fundam.*, **2**, 51 (1963).

11. S. Sourirajan, *Nature*, **199**, 590 (1963).

12. S. Sourirajan and T. S. Govindan, *Proceedings of the First International Symposium on Water Desalination*, Oct. 3–9, 1965, Vol. 1, Washington, D.C., U. S. Dept. of Interior, Office of Saline Water, 1967, pp. 251–274.

13. S. Sourirajan and J. P. Agrawal, Ind. Eng. Chem., **61** (11), 62 (1969).

14. S. Kimura and S. Sourirajan, *A. I. Ch. E. J.*, **13**, 497 (1967).

15. S. Dushman, *Scientific Foundations of Vacuum Techniques*, 2nd ed., Wiley, New York, 1962, Chapt. 2.

16. H. W. Liepmann, *J. Fluid Mech.*, **10**, 65 (1961).

17. R. E. Treybal, Mass Transfer Operations, 2nd ed., McGraw-Hill, New York, 1968, p. 87.

18. G. W. C. Kaye and T. H. Laby, *Tables of Physical and Chemical Constants*, 12th ed., Longmans, London, 1962, pp. 39, 134.

19. R. D. Schultz, S. K. Asunmaa, G. A. Guter, and F. E. Littman, Paper presented at the Second International Meeting, International Society for Neurochemistry, Milan, Italy, Sept. 1–5, 1969.

20. J. P. Agrawal and S. Sourirajan, *J. Appl. Polym. Sci.*, **13**, 1065 (1969).

21. S. A. Stern, T. F. Sinclair, P. J. Gareis, N. P. Vahldieck, and P. H. Mohr, *Ind. Eng. Chem.*, **57** (2), 49 (1965).

Received October 17, 1969
Revised December 4, 1969